IBRACON Structures and Materials Journal
Revista IBRACON de Estruturas e Materiais
ISSN 1983-4195 ismj.org

ORIGINAL ARTICLE

DIC method applied in the calibration of FEA model of rock-mortar cohesive interface

Método DIC aplicado na calibração de um modelo MEF de interface coesiva rocha-argamassa

Edivaldo José Silva Junior[a]
Aref Kalilo Lima Kzam[a]
Julio Florez Lopez[b]

[a]Universidade Federal da Integração Latino Americana, Programa de Pós-graduação em Engenharia Civil de Infraestrutura (PPGECI), Foz do Iguaçu, PR, Brasil
[b]Chongqing University, Chong Qing Shi, Shapingba District, China

Received June 19, 2023
Revised August 08, 2023
Accepted September 26, 2023
Corrected 27 March 2024

Abstract: In civil engineering, the stability of many structures depends on the physical properties of the contact between the concrete seated on the rocky foundation surface. Usually, they are critical structures of great importance to society, such as: bridges, tunnels and dams. Thus, the shear behavior of rock-concrete joints is a key factor of the structural stability. The method of cohesive zones (CZM) allows to simulate the beginning of the formation of a crack and its propagation, without knowing the crack location or when it will start. Thus, in this work, a numerical model was developed capable of simulating the failure due to interfacial delamination of the contact between a structure formed by mortar seated on a rocky granite leaning surface. The calibration of the numerical model was performed using the experimental test results of simple compression on a block of rock in contact with the mortar by an inclined interface. The test was monitored using a high-resolution digital camera. The data were processed using the digital image correlation method (DIC) to obtain displacement data of the laboratory test. The DIC results were used to calibrate the nonlinear numerical model of the test using the bilinear method of cohesive zone in the rock-mortar interfacial contact elements. By a parametric analysis varying the maximum shear stress parameter of the contact cohesive elements, the bilinear law was adjusted (Maximum tensile stress and critical displacement and damage rate). Indirectly, the rate of release of energy of critical deformation from the rupture of the contact was also estimated.

Keywords: interfacial crack, DIC, FEA, Cohesive Zone, Bilinear law, Delamination.

Resumo: Na engenharia civil, a estabilidade de muitas estruturas depende das propriedades físicas do contato entre o concreto assentado na superfície rochosa de fundação. Geralmente são estruturas críticas e de grande importância para a sociedade, tais como: pontes, túneis e barragens. Assim, o comportamento ao cisalhamento das juntas rocha-concreto é um fator chave da estabilidade estrutural. O método das zonas coesivas (MZC) permite simular o início da formação de uma fissura e a sua propagação, sem saber a localização da fissura ou quando esta irá começar. Assim, neste trabalho foi desenvolvido um modelo numérico capaz de simular a ruptura por descolamento interfacial do contato entre uma estrutura formada por argamassa assentada sobre uma superfície inclinada de granito rochoso. A calibração do modelo numérico foi realizada através dos resultados de ensaios experimentais de compressão simples sobre um bloco de rocha em contato com a argamassa por uma interface inclinada. O teste foi monitorado por meio de uma câmera digital de alta resolução. Os dados foram processados utilizando o método de correlação de imagens digitais (CID) para obtenção dos dados de deslocamento do ensaio laboratorial. Os resultados do método CID foram utilizados para calibrar o modelo numérico não linear do ensaio utilizando o método bilinear de zona coesiva nos elementos de contato interfacial rocha-argamassa. Através de uma análise paramétrica variando o parâmetro de tensão cisalhante máxima dos elementos coesivos de contato, determinou-se a lei bilinear ajustada (tensão

Corresponding author: Edivaldo José Silva Junior. E-mail: edivaldo.jsj@gmail.com
Financial support: None.
Conflict of interest: Nothing to declare.
Data Availability: The data that support the findings of this study are openly available in [SILVA JUNIOR - DRIVE] at [https://drive.google.com/drive/folders/1AxWCliIwJyayNxdYAwOde6g8VwO3O7VR?usp=sharing].
This document has an erratum: https://doi.org/10.1590/S1983-41952024000500011

máxima de tração, deslocamento crítico e taxa de dano). Indiretamente, também foi estimada a taxa de liberação de energia de deformação crítica proveniente da ruptura do contato.

Palavras-chave: ruptura interfacial, CID, MEF, Zona Coesiva, Lei Bilinear, Descolamento.

How to cite: E. J. Silva Junior, A. K. L. Kzam, and J. F. Lopez, "DIC method applied in the calibration of FEA model of rock-mortar cohesive interface," *Rev. IBRACON Estrut. Mater.*, vol. 17, no. 5, e17502, 2024, https://doi.org/10.1590/S1983-41952024000500002

1 INTRODUCTION

In civil engineering, the stability of many structures depends on the physical properties of the concrete-rock contact, like bridges and dams. Thus, the shear behavior of joints formed by the settlement of concrete in a rocky interface is a structural stability key factor [1], [2].

Structural numerical simulation allows evaluating the linear and nonlinear behavior of structures such as rock foundations due to technological advances in computation. However, the results obtained from numerical models can be incompatible with the behavior of the real structure or experimental tests. Thus, the Digital Image Correlation method (DIC) is presented as an alternative to establish a connection between the experimental tests results and numerical simulations, allowing to obtain models calibration and validation [3].

DIC method facilitates the extraction of physical quantities from digital images without direct contact with the tested material. This method allows the determination of displacements and deformations of the investigated objects, in two dimensional (2D) and three dimensional (3D) spaces, from high-resolution images that are recorded during a test by image pixel variation [4]. In the case of joints formed by laying concrete on rock, the adhesion occurs during the curing and hardening of the concrete creating a cohesive resistance in contact, preventing displacements.

The CZM allows to model crack propagation and joint detachment without existing crack. Cohesive zone analyzes can predict the locations and directions of early cracks or simulate complex geometries with more than one type of interface. In a ZC (cohesive zone) model, elements are placed along the materials interface. The deformation and separation of these elements under mixed mode loading conditions are guided by tensile separation laws [5].

One of the earliest works related to method of Digital Image Correlation (DIC) was published in 1982 [6], proposing a mathematical approach to convert digitized two-dimensional images into a plane of a specimen undergoing deformations. However, just in 1985, the first experiments were published aiming validating the concepts of the 2D DIC methodology [7]. More refined applications were carried out in 1987 [8]. The work provided estimates of the stress intensity factor on the crack front by a significant computational technology challenge. With technological advancements, the DIC method was more explored as an excellent tool for calibrating numerical models based on deformation field results obtained through monitoring experimental tests.

Due contact behavior between concrete and rock importance in civil engineering, numerous studies have been conducted to investigate the interface interaction of these materials, like shear tests on non-cemented rock-concrete joints subjected to normal loads and under constant stiffness conditions in 1984 [9]. Considering the interface between concrete and rock as weakest zone in an engineering system composed of these two elements [10] investigated the dependence of the fracture behavior of concrete-rock interfaces on the mixed-mode fracture rate (Mode I, II, and III) using experimental and numerical methods. Exploring the technique of Digital Image Correlation (DIC) [11] applied DIC to study the crack propagation process at the concrete-rock interface in two different tests: three-point bending and four-point shear. The obtained results allowed for the analysis of displacement fields, crack width, and propagation length during the fracturing process. The Digital Image Correlation (DIC) technique was used to analyze fracture properties and characterize the length of the Fracture Process Zone (FPZ) in the three-point bending test.

2 DIGITAL IMAGE CORRELATION (DIC)

The DIC method is based on the analysis of successive images, which are obtained before and after the deformation of an object submitted to a load. These images are analyzed by a correlation algorithm that, initially divides the reference image (without deformations) into several sections, called blocks [3]. These sections are mapped and searched by the algorithm in the following image, after deformation [4]. Each block is formed by a unique set of pixels and the objective of the algorithm is to determine its new position after loading. For each section to be unique, the surface of the object must have a high contrast random texture across the interest area. This texture can be natural or artificial, created through random painting using different shapes and gray scales [3]. The DIC methodology has two sources of parameters that must be adjusted and calibrated, distributed in three stages of execution, as shown in Figure 1 [4], [5].

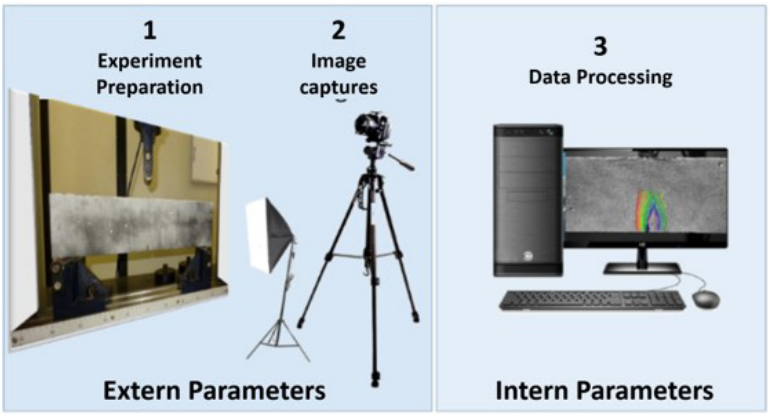

Figure 1. Illustration of DIC steps

Basically, the analyzed interest surface of the object must present a texture allows the visualization of the material's deformation using DIC algorithms [4]. This surface must have a random distribution of grains, high contrast and cover all gray's tone, from level 0 (black) to level 255 (white). It is recommended to use artificial lighting to ensure the same light intensity during all test period. Because the test data is obtained through image capture, DIC processing is extremely sensitive to ambient light variation. In addition, artificial lighting helps to emphasize contrast the texture, improving the accuracy of the results [3].

IMAGES CAPTURE: The test image is captured using a high-resolution digital camera. In the 2D-DIC case, a single Camera is positioned normal to the interest plane [3]. The image acquisition frequency is directly associated with the loading application time and the deformations presented by the object under analysis. The frequency of image capture must be sufficient to map the physical behavior, however, it is not desirable to have an excessive number of images because will only increase the processing time [4].

DATA PROCESSING: From a computational point, monochromatic images have advantages in processing when compared to color images. This is because the intensity of each pixel is defined based using just one scale. In a monochrome image the gray scale ranges from level 0 (black) to 255 (white). In this way, a single matrix is capable storing this information. However, using a color image in RGB (Red-Green-Blue) format, for example, three matrices are needed to define the intensity of each pixel. For this reason, many programs use only monochromatic images [3]. In Figure 2 an illustration of a grayscale image and the respective pixel matrix is presented.

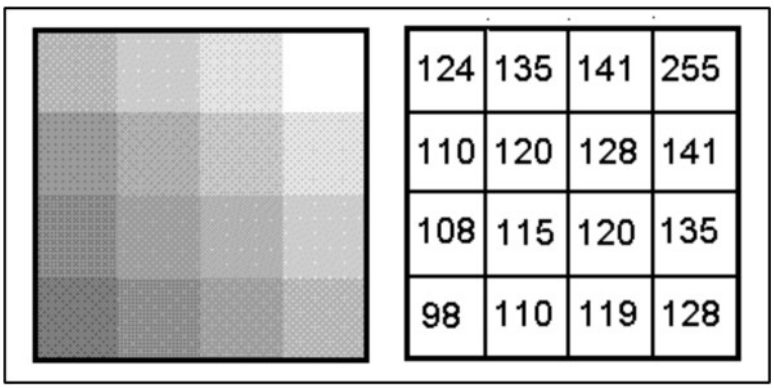

Figure 2. Illustration of a digital image and its respective pixel matrix [12]

After to restrict the interesting area in the reference image and realize a texture validation, it is possible to understand how the DIC algorithms perform the correlation between images through the correspondence of pixel sets, called blocks [3].

Initially, the interesting image area is divided into several small parts with a number of pixels. Each part is called a block. Due to the randomness of the texture, each block haves a unique pixel intensity matrix. Then, for each block in

reference image, the algorithm looks the blocks in the next image until finds the respective matrix by means of a minimization function. If the texture does not present an adequate stochastic pattern, more than one block can present the same tone intensity matrix, causing an incorrect correspondence or even a non-correlation between the images [12].

3 COHESIVE ZONE MODEL

The cohesive zone model (CZM) is an emerging technology capable of simulating a crack formation and propagation. Thus, the advantage of the cohesive zone theory is, it is not necessary to have a started crack point or area. In CZM, interfacial separation occurs within a cohesive damage zone, when the damage exceeds a pre-set limit [5]. Within a cohesive zone (CZ), there are active tensile stresses between surfaces [13]. The interaction is governed by the law of tension separation. Before applying the load, a CZ element is declared healthy (no damage). A completely damaged element means the element was completely separated and does not produce any interaction force between the cohesive surfaces, reaching a damage value equal one. In Figure 3 is illustrated the interfacial separation CZM [5].

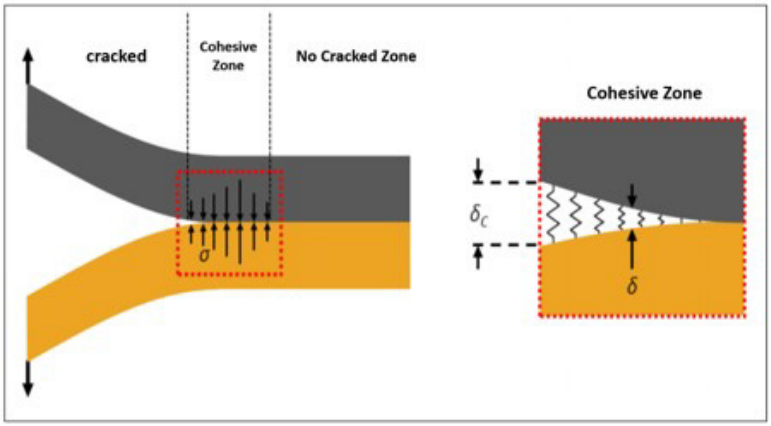

Figure 3. Interfacial separation [5]

3.1 BILINEAR TRACTION-SEPARATION CONSTITUTIVE LAW

The bilinear tensile separation law was introduced in 2001year to model the interfacial separation. Several bimaterial interfaces were simulated using this law [14]. In Figure 4 is presented the bilinear law.

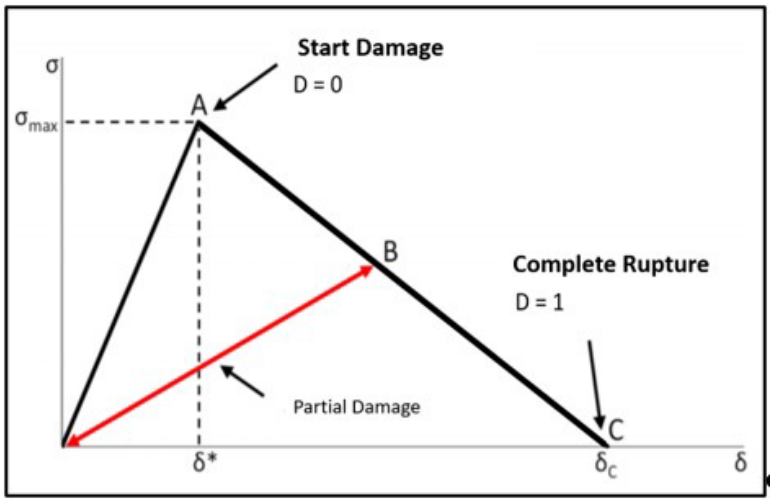

Figure 4. Bilinear tensile separation law for cohesive zone elements [5]

The bilinear law is modeled by the tension (σ) as a function of the interfacial separation (δ). As the CZ elements suffer deformations, they present a linear behavior for $\delta < \delta^*$. In this curve region, no damage is accumulated at the interface and, consequently, unloading results in the CZ returning to original configuration. At point A, the critical tensile stress is reached (σ_{max}), and damage displacement is defined (δ^*) and the damage process starts until arrive the rupture displacement (δ_c). The detachment is monitored as a function of damage parameter (D), calculated by Equation 1. When $\delta > \delta^*$, D increases and, when $\delta \geq \delta_c$, D is maximum, equal 1.

$$D = \begin{Bmatrix} 0 & se\ \delta \leq \delta^* \\ \left(\frac{\delta - \delta^*}{\delta}\right) & se\ \delta^* < \delta < \delta_c \\ 1 & se\ \delta \geq \delta_c \end{Bmatrix} \quad (1)$$

4 MATERIALS AND EXPERIMENTAL PROGRAM

The methodology adopted in this work is shown in Figure 5.

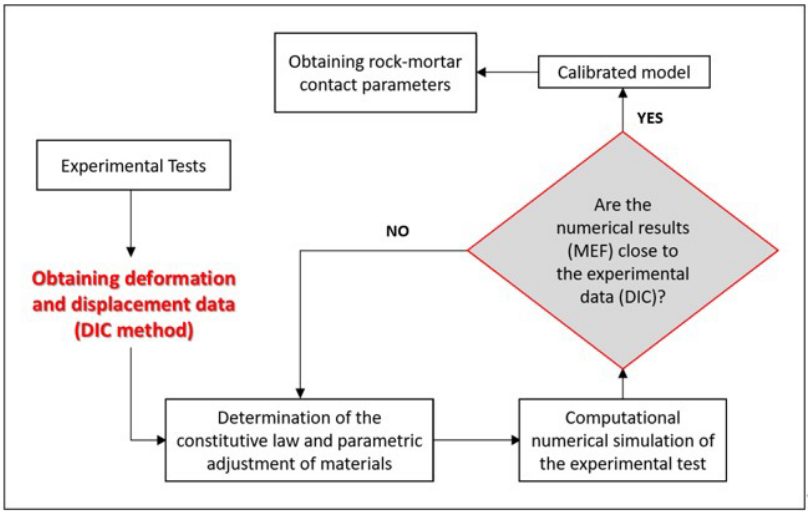

Figure 5. Flowchart of the methodology adopted in this work

According to the availability of the laboratory's infrastructure, it was possible to develop a rock-mortar interface detachment test under normal and shear stresses by a simple axial compression hydraulic press. Figure 6 shows the dimensions of th specimen in millimeters dimensions, as well as the materials of each component. The specimen is subjected to a controlled axial loading at the ends until the rupture of the rock-mortar contact by shear tensile, as shown in Figure 7.

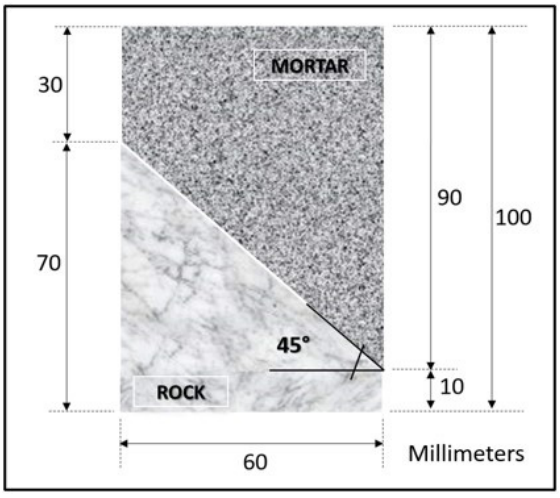

Figure 6. Illustration of the rock-mortar test

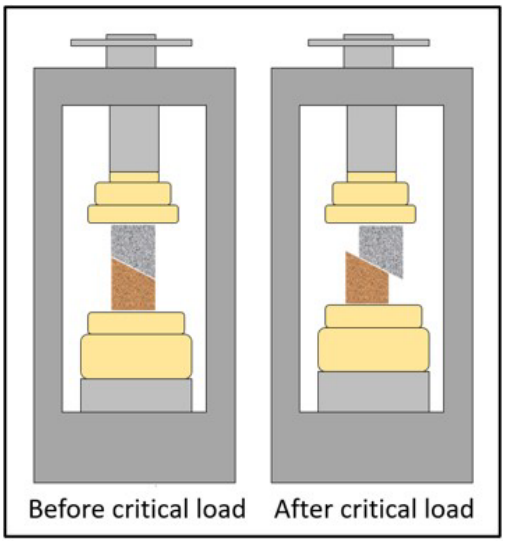

Figure 7. Illustration of the breakage of the rock-mortar contact of the specimen

The equipment used to apply the axial load was the Contenco 100T Digital Electric Hydraulic Press. It has a digital indication system with 5 digits and a resolution of 1 kgf, it also has the maximum peak and tare functions for the load. The equipment allows the application of continuous load and has 2 regulating valves for load increase and decrease, which is controlled by the user following the software recommendation at the time of the test [15].

The camera used was a Sony Alpha a5000 digital camera (Mirrorless Digital Camera ILCE5000L/S), with 20.1 megapixels of resolution [16]. In the Figure 8 is presented the monitoring equipment.

Figure 8. Equipment used for monitoring the surface of interest

Following the DIC specimen preparation method, initially, the specimens receive a layer of white paint. Subsequently, black spray paint was used to create a random fine-grained texture (Figure 9).

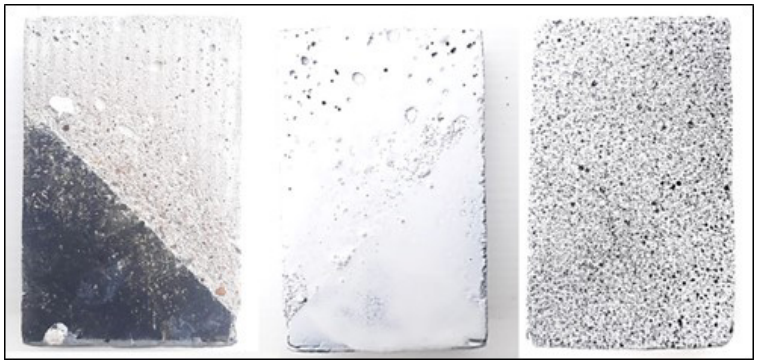

Figure 9. Texture preparation of the rock-mortar specimens

The rupture test of the contact interface between rock and mortar was carried out using a hydraulic press machine. The test was monitored using a Sony Alpha 5000 digital camera (Mirrorless Digital Camera IL-CE5000L/S), with 20.1 megapixels of resolution. In all, six tests were carried out on rock-mortar specimens. In two tests, there was a rupture of the mortar in the central region and a partial rupture of the rock-mortar contact interface (a). In two tests, the total rupture of the contact interface occurred smoothly (b), and, in two tests, the total rupture of the interface occurred abruptly (c), as shown in Figure 10.

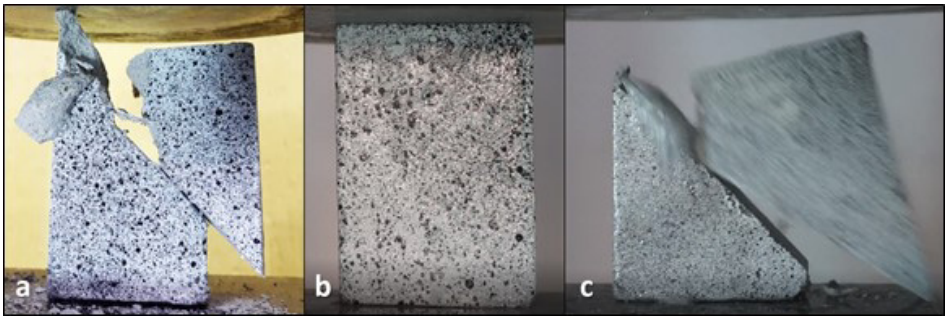

Figure 10. Types of rupture obtained during the tests: partial rupture of the interface (a), smooth total rupture (b) and abrupt total rupture (c)

In Figure 11, the three monitoring points chosen in the specimens to collect displacement data of the images processed by the digital image correlation method are presented. Points 1 and 2 are in the middle of the distance between the bottom and top interface, respectively, and the contact interface. Point 3 is exactly in the middle of the contact interface.

Figure 11. Monitoring Points (DIC)

5 RESULTS AND DISCUSSIONS

5.1 EXPERIMENTAL TEST AND DIC PROCESS TO MONITORING

Figure 12 shows the results of Digital Image Correlation (DIC) processing moments before the laboratory experiment test failure, using the GOM Correlate program.

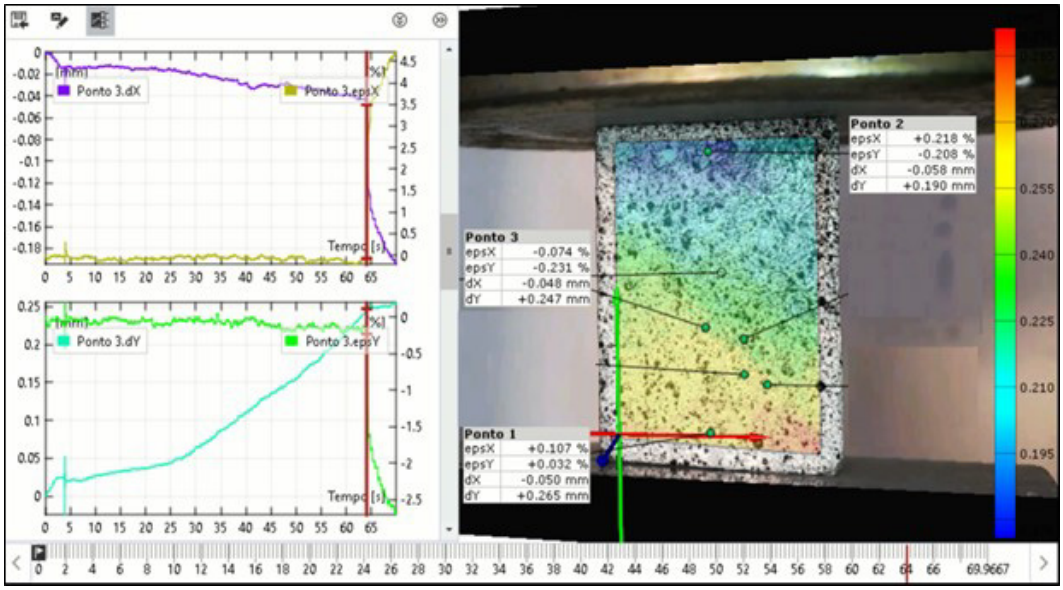

Figure 12. DIC results of vertical displacement field), and three points of displacement and deformation graphs) of the specimen.

In Figure 13 to Figure 15, the displacement results in the vertical (y) and horizontal (x) directions of each monitored point (Figure 11) of test are presented.

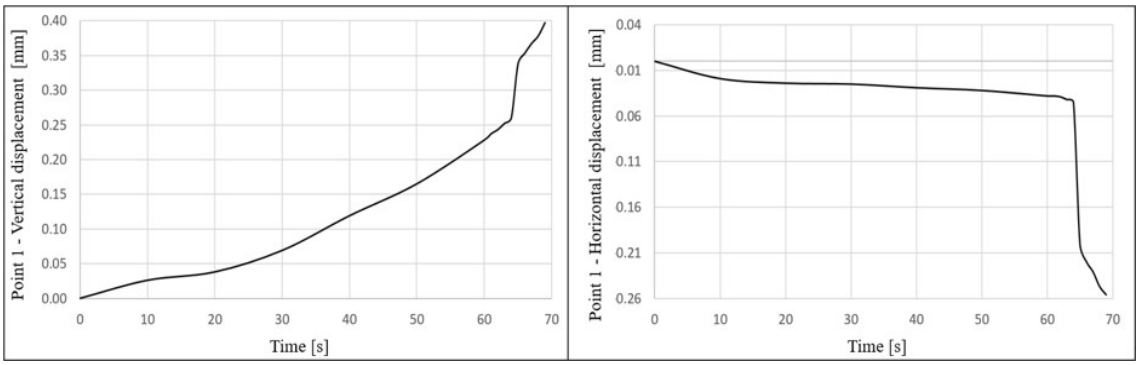

Figure 13. Vertical and horizontal displacement of the experimental test monitoring point 1

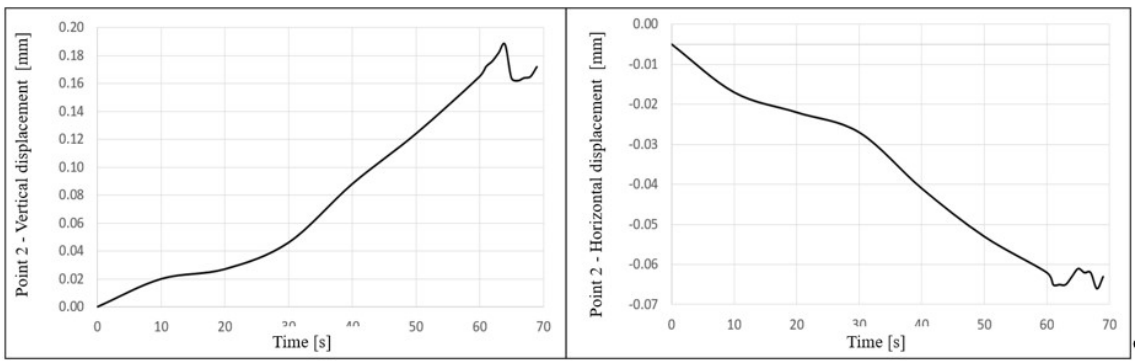

Figure 14. Vertical and horizontal displacement of the experimental test monitoring point 2

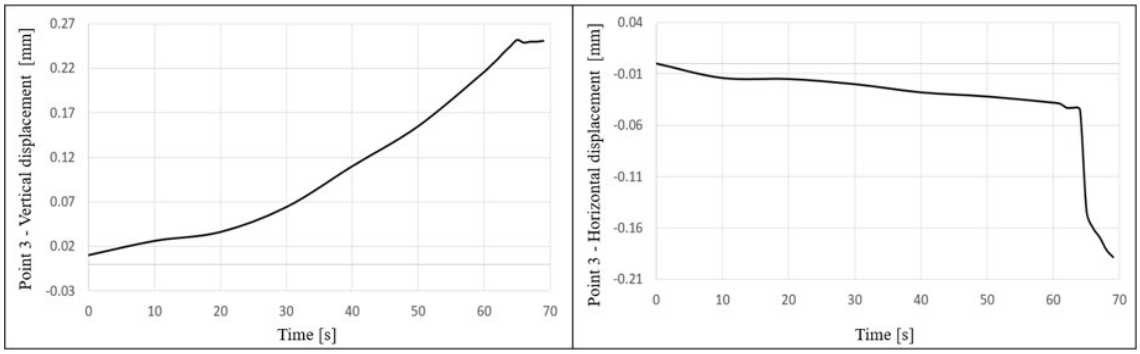

Figure 15. Vertical and horizontal displacement of the experimental test monitoring point 3

5.2 NUMERICAL SIMULATION OF EXPERIMENTAL TEST

To develop the numerical failure model at the rock-mortar contact interface of the specimen using Ansys software [17], it was decided to use the Cohesive Zone Detachment method based on Separation Distance, similar to the Bilinear Law method. In this work, fracture mode II is predominant since the contact interface is compressed all the time during the test. To perform the numerical analysis, it was adopted the materials properties presented in Table 1.

Table 1. Material properties

Material	Modulus of elasticity [GPa]	Poisson's Coefficient	Density [Kg/m^3]
Mortar	21*	0.2*	2350**
Rock	70*	0.25*	2670**

*Properties estimated through DIC results; ** Properties obtained from literature [18].

The mesh is formed by hexahedral elements, solid186. Altogether, the mesh consists of 18,775 nodes and 3,864 elements (Figure 16).

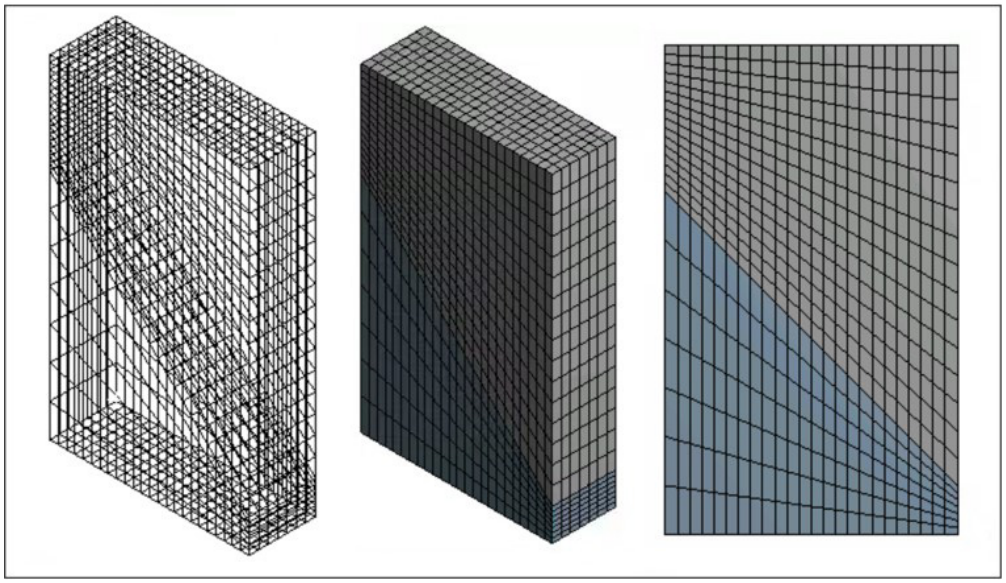

Figure 16. Hexahedral mesh of the numerical model

To simulate the conditions of the hydraulic press, the fix support condition on the upper surface and loading on the lower surface were applied, as shown in Figure 17.

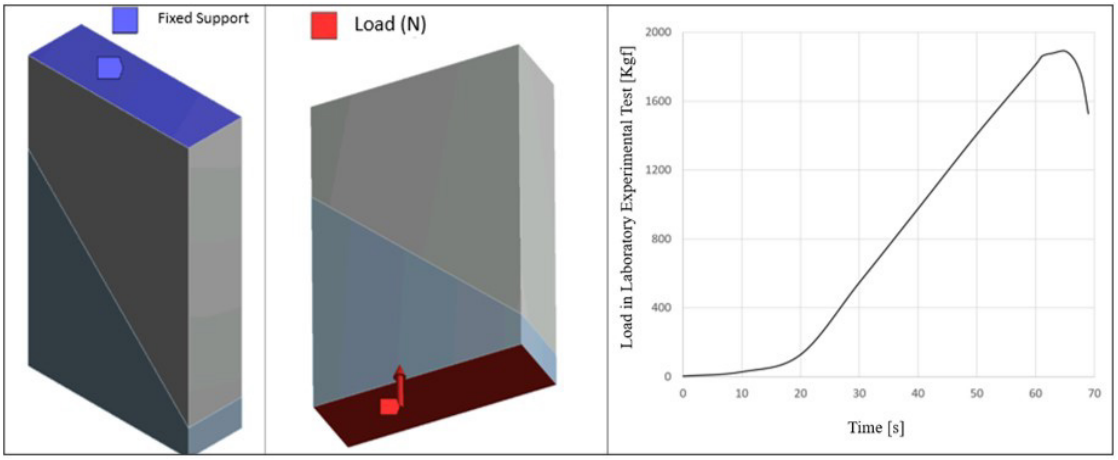

Figure 17. Loading condition of the numerical model according to the experimental test

By the DIC method, aligning the global reference coordinates towards the contact interface, it was found the interface displacement slip of 0.206 mm, milliseconds before rupture, as shown in Figure 18 (t=64.23s). The time of interface rupture moment of the laboratory test can be established by DIC results using the displacement graph abrupt change (Figure 15).

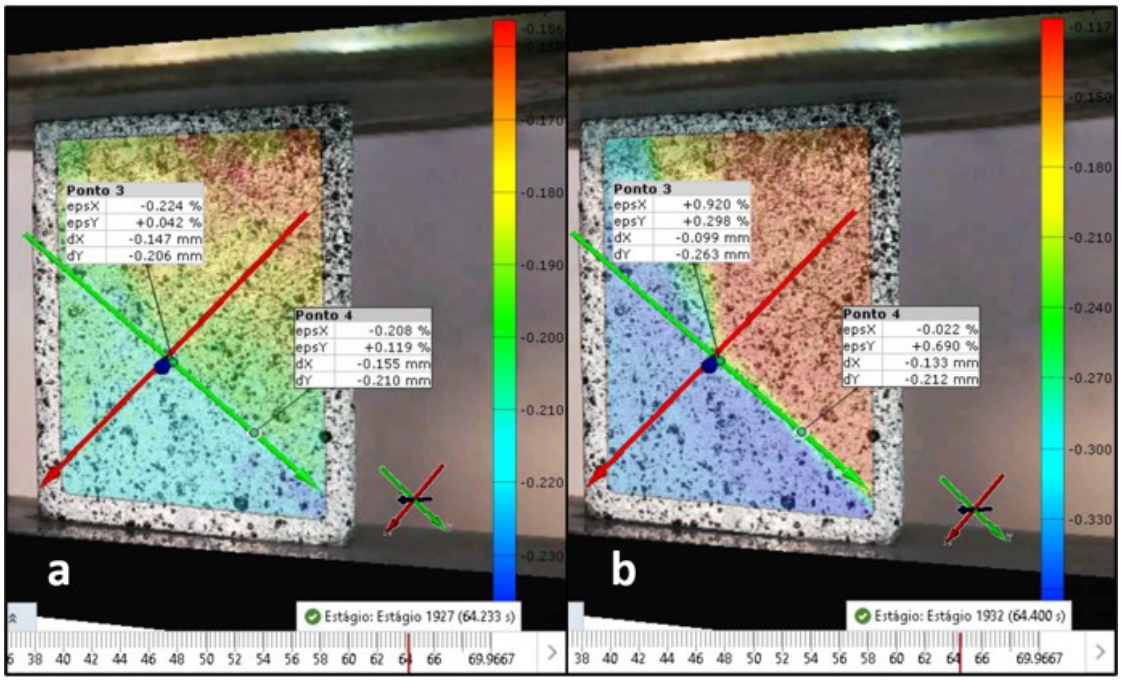

Figure 18. Contact interface displacement slip analysis obtained by DIC method before (a) and after (b) rupture

Finally, to start the nonlinear analysis and define the cohesive zone parameters through the bilinear law, the rupture displacement equal to 0.2 mm was defined, to the time t= 64.2s) as presented in the experimental test and monitored by the DIC method (Figure 18). Figure 19 shows the partially developed Bilinear Law for Cohesive Zones to the experiment numerical simulation.

To define the remaining properties of the bilinear law, a parametric analysis was performed varying the maximum shear stress parameter until the model rupture occurs at time t = 64.2 seconds, like laboratory experiment (figure 18). The Table 2 presents the main results of the parametric analysis realized changing maximum shear stress parameter until obtaining the same behavior of the numerical model and calibrating it with the experimental DIC results.

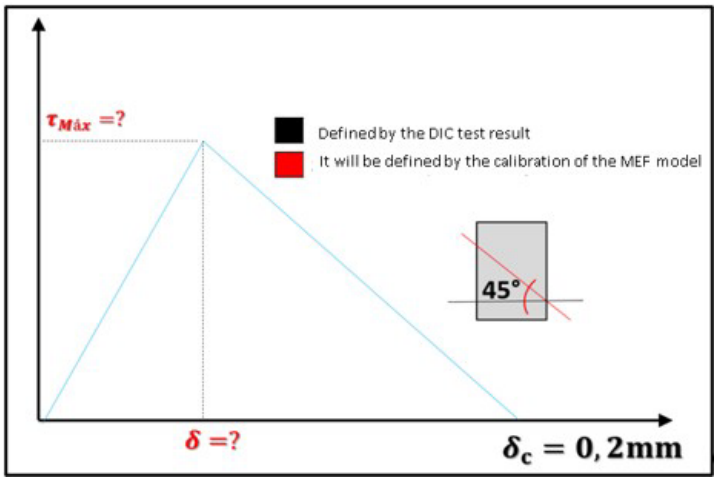

Figure 19. Graphic illustration of the Bilinear Law partially defined

Table 2. Summary of the parametric analysis performed to calibrate the numerical model

N°	$\tau_{máx}$ [MPa]	$\delta_{máx}$ [mm]	Damage start time [seconds] ($\tau_{contato} > \tau_{máx}$)	Total break time [seconds] ($\delta_{contato} > \delta_{máx}$)
1	11,3	0.2	60	-
2	10	0.2	55	-
3	8	0.2	48	67
4	7,5	0.2	46	66
5	7,2	0.2	45.5	64.4
6	**7,15**	**0.2**	**45.4**	**64.2**

In Figure 20 and Figure 21, the vertical displacement (Y), experimental test (DIC) and Finite Element Analysis (FEA) fields are shown, before and after the crack failure, respectively.

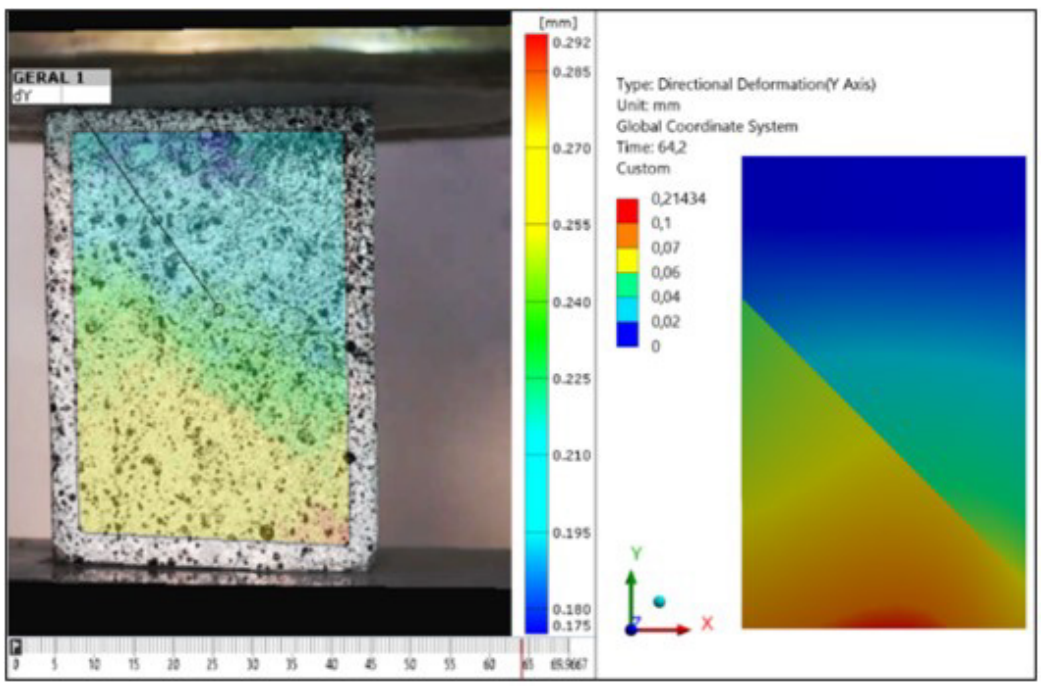

Figure 20. Test vertical displacement field, DIC and numerical model (t=64.2s)

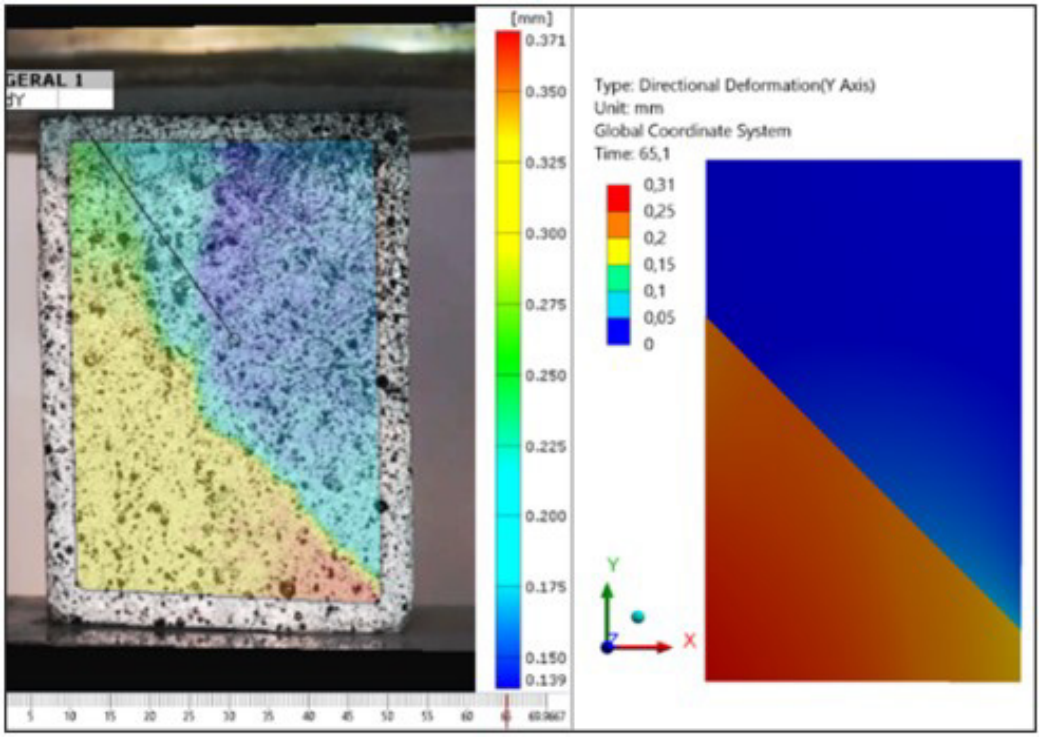

Figure 21. Test vertical displacement field, DIC and numerical model (t=65.1s)

In Figure 22 and Figure 23, the fields of horizontal displacement (X), the experimental test (DIC) and the numerical model are presented.

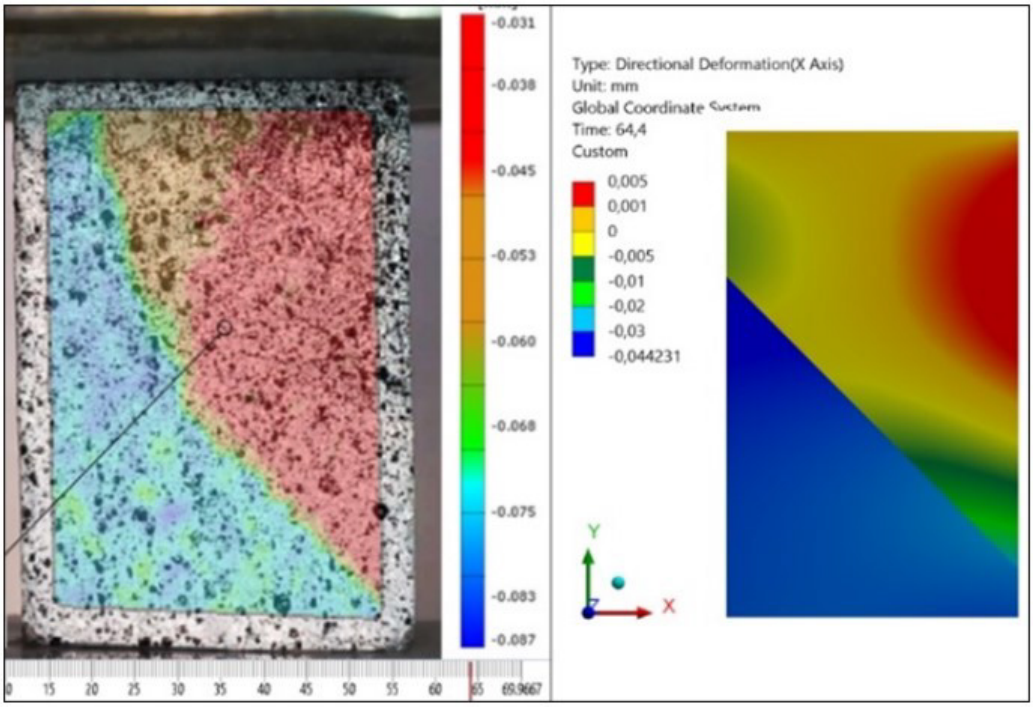

Figure 22. Test Horizontal Displacement Field, DIC and Numerical Model (t=64.2s)

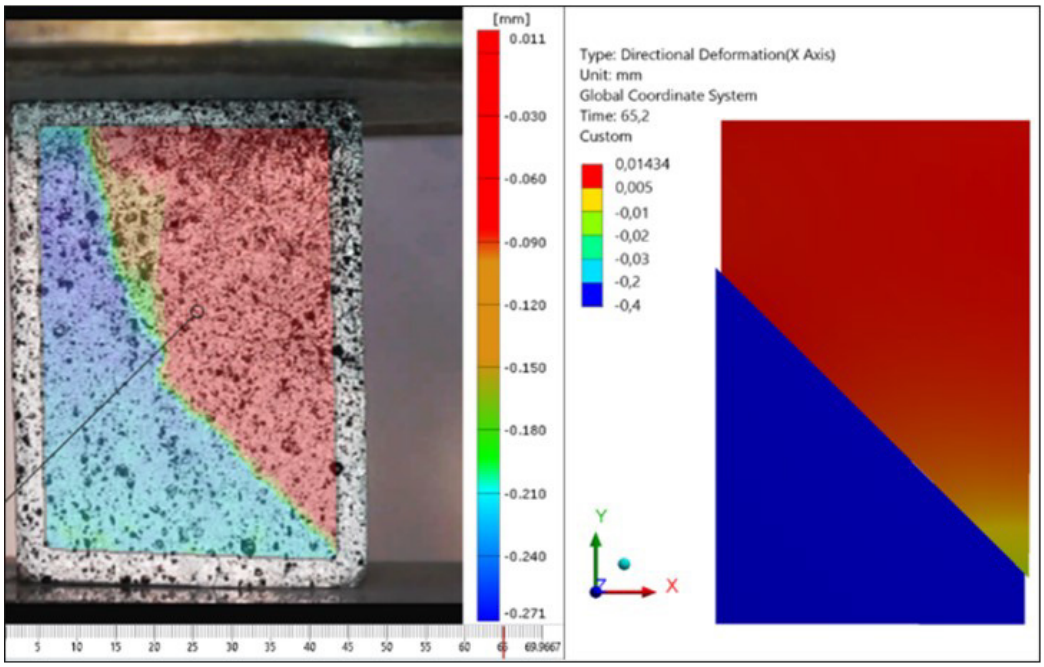

Figure 23. Test Horizontal Displacement Field, DIC and Numerical Model (t=65.1s)

The analysis of the monitoring points of the experimental test was carried out and compared with results from the same points of the numerical model. Graphic illustrations of the monitoring points, DIC and FEA, are shown in Figure 24 to Figure 26.

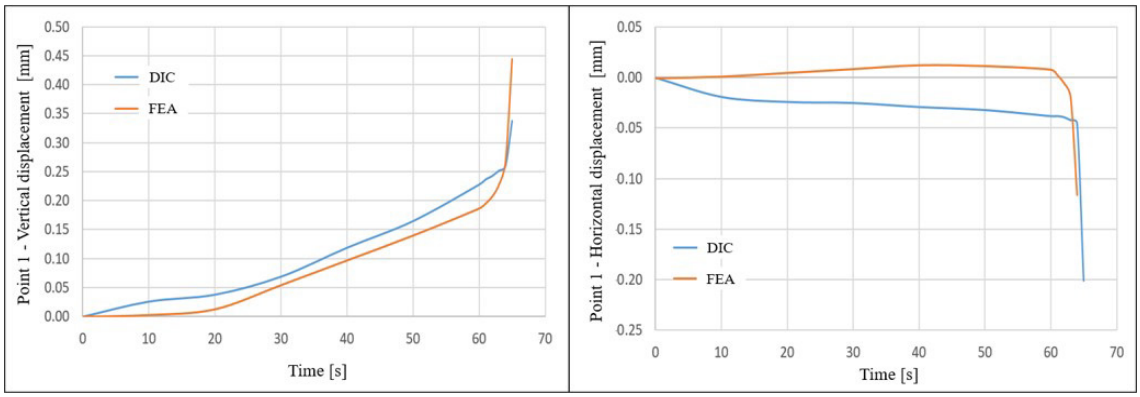

Figure 24. Vertical and horizontal displacements of monitoring point 1

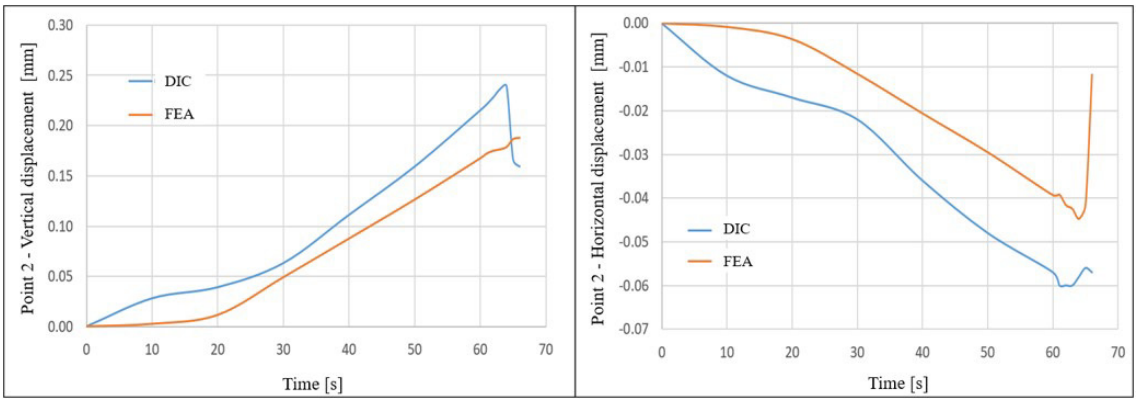

Figure 25. Vertical and horizontal displacements of monitoring point 2

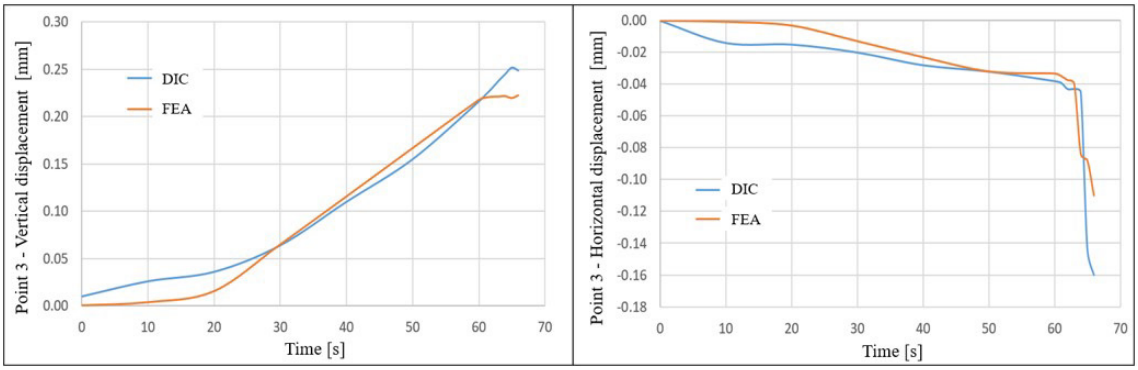

Figure 26. Vertical and horizontal displacements of monitoring point 3

The analysis of the accumulated percentage difference of the DIC and FEA results was carried out using MAPE (Mean Absolute Percentage Error). Table 3 shows the MAPE values for each monitoring point.

Table 3. MAPE error of monitoring points

Monitored point	**1**		**2**		**3**	
Displacement direction	x	y	x	y	x	y
MAPE Error	-	11.77	36.59	19.5	5.94	3.06

5.3 CONTACT INTERFACE BEHAVIOR (COHESIVE ZONE - BILINEAR LAW)

Calibrating the numerical model with the CZM properties presented in Table 2, it can be seen in Figure 27 and Figure 28a, the nonlinear behavior in the contact starts at the same moment that the maximum shear stress of the interface reaches the maximum value of the shear Bilinear Law, 7.15 MPa (t=45.4 seconds).

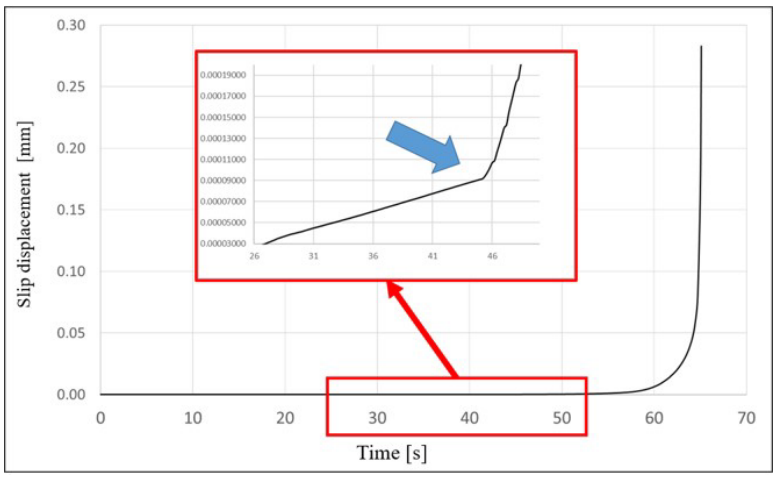

Figure 27. Sliding of the contact and detail interface when non-linear behavior starts

Thus, from time t=45.4s, the process of damage to the contact elements began. The total breakage of the contact occurs at time t=64.2s, when most of the contact elements reach the maximum displacement provided for in the Bilinear Law of 0.2 mm. Analyzing the maximum shear stress field at the contact interface, it is observed that the region with the highest value moves from the upper left region (t=45.4s) to the lower right region (t=64.2s). At the failure moment, the contact interface has a maximum shear stress of 14.5 MPa, as shown in Figure 28b. This is because, with the beginning of the detachment of the contact interface, the distribution area of stress decreases. In this way, the shear stress increases at the same speed as the contact detachment occurs, until total rupture.

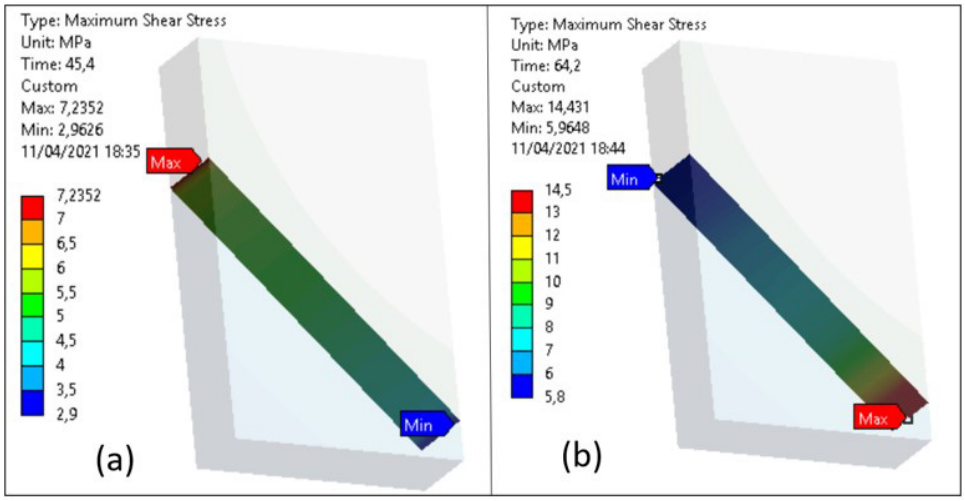

Figure 28. Maximum shear stress field at the contact interface: (a) t=45.4s and (b) t=64.2s

5.4 COHESIVE ZONE PARAMETERS DETERMINATION

The bilinear law is defined by three parameters: maximum stress, critical displacement and loading and unloading rate [14]. The latter is obtained through the relationship between the displacement that initiates the damage and the critical displacement. Analyzing Figure 27, it is possible to observe that the damage starts when the contact element reaches the maximum shear stress $\tau_{max} = 7.15\ MPa$ and displacement $\delta^* = 9 \times 10^{-5}\ mm$. Thus, the parameters of the Bilinear Law that simulate the behavior of the rock-mortar cohesive interface of the experimental test (with a 45º contact interface inclination angle) are presented in Figure 29.

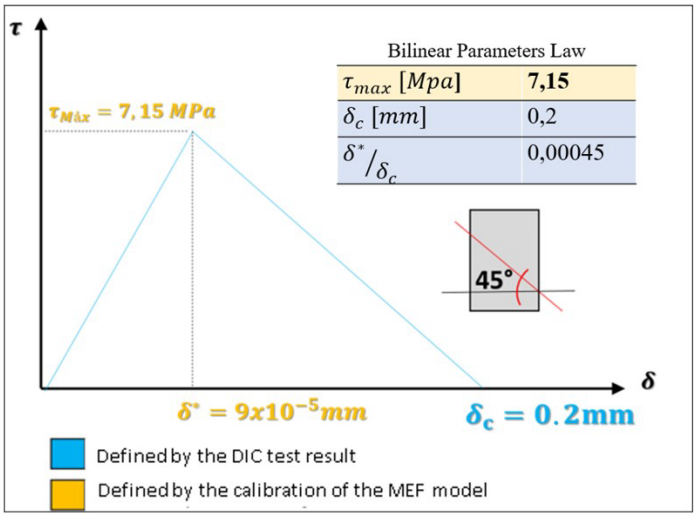

Figure 29. Graphic illustration of the complete bilinear law [19].

When a finite element begins to break down, the area below the tensile separation law function accounts for the mechanical work required to separate the element. Thus, the area under the curve is equivalent to the Gc (critical rate of deformation energy release of linear elastic fracture mechanics) [5]. Using the parameters of the Bilinear law, Gc can be estimated using Equation 2.

$G_c = \frac{1}{2}\delta_c \sigma_{max}$. Thus, the Gc parameter is equal to 0.71 [N/mm]. (2)

6 CONCLUSIONS

In this work, the application of the DIC method presented several challenges, such as the granular texturing of prismatic specimens. Due to the size of the specimen and the available digital camera for image capture, it was decided to use spray paint for texturing. The technique was applied by lightly pressing the spray button, creating a splatter effect. The second challenge was related to image capture speed. To record the contact interface displacement phenomenon, it was necessary to capture by video record. This decision impacted the DIC processing phase. Using a computer with 56 GB of RAM and an Intel i5 3.50 GHz processor, the processing time for the conducted tests was 40 to 60 minutes.

Due to the difficulty to simulate precisely experimental test motion, in addition to the numerical simplifications adopted, such as isotropy and material homogeneity, it was decided to monitor points near the central region of the specimens, including the rock-mortar contact interface. After conducting the test and processing the images, a linear elastic analysis of the numerical model was performed to evaluate the behavior of the contact interface at time t=64.2s (moment of experimental test failure). The results showed an average slip and a maximum shear stress at the contact interface of 1.53e-5 mm and 11.3 MPa, respectively.

Through the DIC method, by aligning the reference coordinates along the contact interface direction, it was observed that the interface exhibited a displacement of 0.206 mm, milliseconds before rupture. Thus, it was concluded that, during the axial compression test, the contact interface of the specimen did not exhibit linear elastic behavior until the moment of rupture (t=64.233s). The process of damaging this interface started seconds before reaching the maximum shear stress, which should be less than 11.3 MPa.

Regarding the nonlinear numerical contact model, after evaluating all available cohesive zone methods in the Ansys material library, the Separation-based Cohesive Law was chosen for use. Subsequently, a parametric analysis was conducted by varying the maximum shear stress parameter of the contact cohesive elements to calibrate the numerical model considering the exact test failure time as one of the requirements for simulation validation.

Using the presented cohesive zone parameters in Figure 29, the numerical model initiated the damaging process of the contact elements at time t=45.4s, reaching the predicted maximum shear stress in the bilinear law (7.15 MPa). The complete rupture of contact occurred at time t=64.2s, where most of the contact elements reached the maximum displacement of 0.2 mm.

Analyzing the maximum shear stress field at the contact interface, it was observed that the region with the highest value translated from the upper left side of the specimen (t=45.4s) to the lower right side (t=64.2s), traversing the entire contact interface during this period. At the moment of rupture, the lower region on the right side of the contact interface exhibited a maximum shear stress of 14.5 MPa. This occurs because, with the onset of contact interface rupture, the stress distribution area decreases. Therefore, the shear stress increases at the same rate as the contact separation until total rupture occurs, at which point the maximum shear stress tends to infinity, and the simulation is interrupted. Subsequently, comparative analyses were performed between the DIC and FEM results of the monitoring points, including the analysis of accumulated error throughout the test using the MAPE error. Overall, the highest MAPE errors are related to the horizontal displacement of the monitored points. The MAPE error of the horizontal displacement of point 1 was not tabulated due to the significant difference between the DIC and FEM results. An explanation may be the location of the monitoring point. Point 1 is close to the bottom surface of the specimen. In this region, the press platform is elevated for loading. The equipment used for the test has an analog load increment system controlled by the user. Therefore, variations in loading speed may have caused abrupt variations in the platform displacement and consequently decreased the precision of the DUC results in this region.

Overall, the accumulated difference throughout the test is considered satisfactory, particularly in the contact interface region where the MAPE error for horizontal displacement was 5.94%, and for vertical displacement, 3.06%. Finally, with the considered calibrated model, the Bilinear Cohesive Zone Law was defined for the specific case of a 45° contact interface between rock and laboratory-tested mortar.

ACKNOWLEDGEMENTS

The authors would like to thank UNIAMERICA for Civil Engineering laboratory support, FPTI for ANSYS software license, and UNILA for PPECI professors' support.

7 REFERENCES

[1] M. H. Tian, W. Z. Chen, D. S. Yang, and J. P. Yang, "Experimental and numerical analysis of the shear behavior of cemented concrete–rock joints," *Rock Mech. Rock Eng.*, vol. 48, pp. 213–222, Jan 2015, http://dx.doi.org/10.1007/s00603-014-0560-6.

[2] Z. Hong, T. Ean, S. Chongmin, D. Tao, L. Gao and L. Hongjun, "Experimental and numerical study of the dependency of interface fracture in concrete-rock specimens on mode mixity," *Eng. Fract.Mech.*, vol. 124-125, pp. 287-309, 2014, https://doi.org/10.1016/j.engfracmech.2014.04.030.

[3] H. Schreier, J. J. Orteu, and M. A. Sutton, *Correlation for Shape, Motion and Deformation Measurements: Basic Concepts, Theory and Applications*. USA: Springer Science, 2009.

[4] G. Almeida, F. Melicio, C. Chastre, and J. Fonseca, "Displacement measurements with ARPS in T-beams load tests," in *Technological Innovation for Sustainability. DoCEIS 2011. IFIP Advances in Information and Communication Technology*, L. M. Camarinha-Matos, Ed., Berlin, Heidelberg: Springer, 2011, vol. 349, pp. 286-293. https://doi.org/10.1007/978-3-642-19170-1_31.

[5] W. E. R. Krieger, S. Raghavan, and S. K. Sitaraman, "Experiments for obtaining cohesive-zone parameters for copper-mold compound interfacial delamination," *IEEE Trans. Compon. Packaging Manuf. Technol.*, vol. 6, no. 9, pp. 1389-1398, 2016, http://dx.doi.org/10.1109/TCPMT.2016.2589223.

[6] W. H. Peters and W. F. Ranson, "Digital imaging techniques in experimental stress analysis. *Opt. Engineergin.*, vol. 21, no. 3, pp. 213427, 1982, http://dx.doi.org/10.1117/12.7972925.

[7] T. C. Chu, W. F. Ranson, M. A. Sutton and W. H. Peters, Applications of digital image-correlation techniques to experimental mechanics," *Exp. Mech.*, vol. 21, no. 3, pp. 232-244, 1985.

[8] S. R. McNeilli, W. H. Peters, and M. A. Sutton, "Estimation of stress intensity factor by digital image correlation," *Eng. Fract. Mech.*, vol. 28, no. 1, pp. 101-112, 1987, http://dx.doi.org/10.1016/0013-7944(87)90124-X.

[9] W. Johnstone and T. S. K. Lam, Frictional characteristics of planar concrete–rock interfaces under constant normal stiffness condition, in *4th Australia–New Zealand Conf. Geomechanics*, Perth, Australia, 1984, pp. 397-401. https://www.issmge.org/uploads/publications/89/91/4ANZ_071.pdf

[10] Z. Hong, T. Ean, S. Chongmin, D. Tao, L. Gao, and L. Hongjun. Experimental and numerical study of the dependency of interface fracture in concrete-rock specimens on mode mixity *Eng. Fract. Mech.*, vol. 124-125, pp. 287-309, 2014, http://dx.doi.org/10.1016/j.engfracmech.2014.04.030.

[11] D. Wei, W. Zhimin, M. Z. Xinag, W. Na, and G. Kastiukas, "An experimental study on crack propagation at rock-concrete interface using digital image correlation technique," *Eng. Fract. Mech.*, vol. 171, pp. 50–63, 2017, http://dx.doi.org/10.1016/j.engfracmech.2016.12.003.

[12] A. Silva, "Correlação de imagens digitais em ensaios de compressão diametral em rochas," Tese de doutorado. Univ. Fed. Minas Gerais, Belo Horizonte, 2019. [Online]. Available: https://repositorio.ufmg.br/handle/1843/30275

[13] F. M. Mukhtar, A. Jawdhari and A. M. Peiris, "Mixed-Mode FRP–concrete bond failure analysis using a novel test apparatus and 3D nonlinear FEM," *J. Compos. Constr.*, vol. 26, no. 6, pp. 1090-0268, 2022, http://dx.doi.org/10.1061/(ASCE)CC.1943-5614.0001274

[14] G. Alfano and M. Crisfield, "Finite element interface models for the delamination analysis of laminated composites: mechanical and computational issues," *Int. J. Numer. Methods Eng.*, vol. 50, no. 7, pp. 1701–1736, 2001, http://dx.doi.org/10.1002/nme.93.

[15] CONTENCO, *Electric Hydraulic Press, Capacity 100 Tf – Technical Specification*, 2023. Available: https://contenco.com.br/produto/prensa-hidraulica-eletrica-digital-100t-i-3025-b/ (accessed June 19, 2023).

[16] SONY, *ILCE-5000 Digital Camera - Full Specifications and Features*, 2023. Available: https://www.sony.pt/electronics/camaras-lentes-amoviveis/ilce-5000-kit/specifications (accessed June 19, 2023).

[17] ANSYS, *Release 21 R1 Documentation for ANSYS*. Canonsburg, PA: ANSYS, 2021.

[18] C. C. Santos, D. C. C. Dal Molin, G. C. Isaia, and J. R. Masuero, "Effects of coarse aggregates shape and modulus of elasticity, mix design parameters and their interactions on concrete modulus of elasticity," *Rev Mater*, vol. 27, n. 1, pp. e13155, 2022, https://doi.org/10.1590/S1517-707620220001.1355

[19] E. J. Silva Junior, "Método CID Aplicado na Calibração de Modelo MEF de Descolamento de Interface Coesiva Rocha-argamassa", Dissertação de mestrado. Prog. Pós-grad. Eng. Civ. Infraestrutura, Univ. Fed. Integração Latino Americana, Foz do Iguaçu, 2021 [Online]. Available: https://bdtd.ibict.br/vufind/Record/UNIL_2b2dc08964a83095988e15664215235d

Author contributions: EJS Jr: conceptualization, Methodology, Data curation, Investigation, Resources, Writing – original draft; AKLK: Supervision, Validation, Writing – review & editing; JFL: Conceptualization, Methodology, Supervision, Validation.

Editors: Vladimir Haach, Guilherme Aris Parsekian.